Simultaneous Radio Occultation for Intersatellite Comparison of Bending Angles toward More Accurate Atmospheric Sounding

CHANGYONG CAO,[a] WENHUI WANG,[b] ERIN LYNCH,[b] YAN BAI,[b] SHU-PENG HO,[a] AND BIN ZHANG[b]

[a] *NOAA/NESDIS/STAR, College Park, Maryland*
[b] *Cooperative Institute for Satellite Earth System Studies, Earth System Science Interdisciplinary Center, University of Maryland, College Park, College Park, Maryland*

(Manuscript received 16 March 2020, in final form 8 October 2020)

ABSTRACT: Global Navigation Satellite System (GNSS) radio occultation (RO) is a remote sensing technique that uses International System of Units (SI) traceable GNSS signals for atmospheric limb soundings. The retrieved atmospheric temperature profile is believed to be more accurate and stable than those from other remote sensing techniques, although rigorous comparison between independent measurements is difficult because of time and space differences between individual RO events. Typical RO comparisons are based on global statistics with relaxed matchup criteria (within 3 h and 250 km) that are less than optimal given the dynamic nature and spatial nonuniformity of the atmosphere. This study presents a novel method that allows for direct comparison of bending angles when simultaneous RO measurements occur near the simultaneous nadir overpasses (SNO) of two low-Earth-orbit satellites receiving the same GNSS signal passing through approximately the same atmosphere, within minutes in time and less than 125 km in distance. Using this method, we found very good agreement between Formosa Satellite 7 (FORMOSAT-7)/second Constellation Observing System for Meteorology, Ionosphere and Climate (COSMIC-2) satellite measurements and those from *MetOp-A*/*B*/*C*, COSMIC-1, *Korea Multi-Purpose Satellite 5* (*KOMPSAT-5*), and *Paz*, although systematic biases are also found in some of the intercomparisons. Instrument and processing algorithm performances at different altitudes are also characterized. It is expected that this method can be used for the validation of GNSS RO measurements for most missions and would be a new addition to the tools for intersatellite calibration. This is especially important given the large number of RO measurements made available both publicly and commercially, and the expansion of receiver capabilities to all GNSS systems.

KEYWORDS: Atmosphere; Remote sensing; Soundings

1. Background and previous studies

The Global Navigation Satellite System (GNSS) is the extension of the well-known global positioning system (GPS) that enables the determination of the precise geolocation of any point on the globe. The GPS constellation consists of ~30 operational satellites in medium-Earth orbit (MEO) at an altitude of ~20 000 km, circling Earth every ~12 h. Other GNSS systems include Russia's Global Navigation Satellite System (GLONASS), Europe's Galileo, Japan's Quasi-Zenith Satellite System (QZSS), and China's Beidou Navigation Satellite System (BDS). The basic principle of GPS positioning relies on active microwave signals transmitted at ~1.2–1.5-GHz frequency where the atmospheric absorption is relatively small. Typically, two frequencies, L1 and L2, are used to isolate the effect from the ionosphere. Nevertheless, the atmosphere still affects the signal at the receiver end, which introduces uncertainties in geolocation accuracy known as "atmospheric effects" to the geodesists. This unwanted "noise" fortunately becomes the important "signal" in radio occultation studies because as the signal passes through the atmosphere, the traveling signal is "bent" along the path (thus the term bending angle) where it is received by a satellite in low-Earth orbit (LEO). The path of the signal is bent by gradients in atmospheric refractivity that delay the arrival of the GNSS signal at the receiver as it propagates through a longer path. The difference between the direct geometric distance separating the GNSS and LEO satellites and the arc distance along the bending path becomes the extra time that it takes (expressed as excess phase) from which the bending angle is derived (Kursinski et al. 1997).

Radio occultations occur only when the GNSS and LEO satellites are in a configuration such that the signal path slices through the atmosphere at different altitudes as an LEO satellite equipped with a GNSS receiver rises above or sets below the disk of Earth. Because of the unique configuration of such events in a four-dimensional space, it is difficult to independently verify the measurements through comparisons with close matchups. On the other hand, there is a need to verify the quality of the measurements and inversion algorithms because a number of instrument related factors such as clock drift, algorithm, receiver firmware, hardware, and signal to noise ratio may affect the accuracy of the bending angle as well as the atmospheric profile retrievals.

Three types of radio occultation (RO) intercomparison approaches can be found in the published literature. Schreiner et al. (2007) and Ho et al. (2009) studied the RO precision using the method of coplanar comparisons between the six satellites in the first Constellation Observing System for Meteorology, Ionosphere and Climate (COSMIC-1) constellation. This approach takes advantage of the RO constellation shortly after launch when the six satellites were still in the same orbital plane following each other closely, providing excellent opportunities for near-simultaneous RO of the same atmosphere

Corresponding author: Changyong Cao, changyong.cao@noaa.gov

DOI: 10.1175/JTECH-D-20-0036.1

within 10 km. This allows direct comparisons of bending angle and refractivity to quantify the instrument performance where the exact same GNSS signals passing through the same atmosphere are detected by two GNSS receivers that are very close to each other. With the launch of Formosa Satellite 7 (FORMOSAT-7)/COSMIC-2 (hereinafter COSMIC-2) in June 2019, the same method has been used to analyze early orbit data by the COSMIC-2 calibration/validation working group (Schreiner et al. 2020; Ho et al. 2020, manuscript submitted to *Remote Sens.*). The disadvantages of this method are that the ideal orbital configuration only exists within a short period of time after launch, followed by orbital phasing that puts the satellites in different orbital planes. Also, the early orbit data may have uncertainties since all postlaunch issues have yet to be uncovered and fully addressed by software, firmware, and parameter updates performed in postlaunch calibration/validation. Another limitation is that the coplanar method can only be used for multisatellite GNSS RO missions.

The second approach is to compare collocated profiles between two RO missions where the RO–RO matchup is typically within a 1-h time window and 250–300 km in distance (Anthes et al. 2008; Ho et al. 2010a,b). The disadvantages of this approach are that the received signals are emitted from different GPS emitters and the signals traveling along different atmosphere paths are compared. One has to assume a homogenous atmosphere that does not change significantly with time in the comparison. Additionally, large sample numbers are usually needed in this type of comparison.

The third method compares RO measurements with other data such as in situ measurements by radiosondes, where the matchup criteria is typically a 3-h time window and 250-km distance, or model-generated data such as those from the European Centre for Medium-Range Weather Forecasts (ECMWF) weather model (Ho et al. 2010a,b, 2017, 2019; Schreiner et al. 2020). Global statistics are generated to evaluate the differences. However, in this approach, it is difficult to separate the instrument performance from model or observation uncertainties, since it is recognized that, while radiosondes often serve as the ''ground truth,'' the measurements also inherit uncertainties and limitations in the radiosonde system themselves (Sun et al. 2019). Numerical weather prediction (NWP) models also have their own uncertainties and biases. Nevertheless, since the RO bending angles are directly assimilated in numerical weather models, the agreement between them is of great interest to both the RO and NWP communities and has been used in the validation of RO measurements such as in the COSMIC-2 postlaunch calibration/validation.

In this study, we introduce a new method for direct comparison of RO bending angles from a pair of LEO satellites near the simultaneous nadir overpass (SNO), named RO@SNO. Similar to SNO comparisons for nadir-viewing sounders, the RO@SNO approach explores simultaneous limb sounding when two LEO RO receivers are close to each other (although not at the same altitude) while receiving the same GNSS signal through approximately the same atmospheric path. This approach is different from the three methods discussed above because 1) this method is an extension of the SNO method (Cao et al. 2004, 2005; Iacovazzi and Cao 2007; Wang et al. 2011) for RO limb-sounding applications where it utilizes simultaneous RO measurements from LEO satellites in different orbital planes; 2) it allows for the direct comparison of bending angles from signals along nearly identical atmospheric path, emitted by the same GNSS transmitter, since the measurements are collected at nearly the same time and location by the satellite pair; and 3) the comparison scenario occurs periodically as long as the satellite orbital altitude difference exists, which makes long-term comparisons possible. We believe that this method complements the traditional approaches for RO data comparisons. Sample data produced by the TriGNSS Radio Occultation System (TGRS) on COSMIC-2, Global Navigation Satellite System Receiver for Atmospheric Sounding (GRAS) on *MetOp-A*/*B*/*C*, and Integrated GPS Occultation Receiver (IGOR) on COSMIC-1, *Korea Multi-Purpose Satellite 5* (*KOMPSAT-5*), and *Paz* are used to demonstrate the usefulness of this method. In the following, we present the method in section 2 and discuss the dataset used for the study in section 3. Results and discussion are presented in section 4, and the conclusions are provided in section 5.

2. Method

The SNO method for intersatellite calibration is well studied and demonstrated (Cao et al. 2004, 2005; Cao and Heidinger 2002), and it has been successfully used for the intersatellite calibration of most Earth observation satellite instruments, from ultraviolet, visible, and infrared, to microwave radiometers (Iacovazzi and Cao 2007; Zou et al. 2006; Wang et al. 2011). The method has been adopted by the World Meteorological Organization (WMO) Global Space-Based Intercalibration System (GSICS) as one of the cornerstones for intersatellite calibration. A brief overview of this method is included here for reference.

From Kepler's laws of planetary motion, given two Earth-orbiting satellites at different altitudes, there is an orbital period difference between them that accumulates over time and eventually allows the lower altitude satellite to ''catch up'' with the one at higher altitude, resulting in an SNO event at the orbital intersection. The time and distance criteria used for SNO intercalibration are typically within 30 s and 10 km, although a trade-off can be made between number of events and more relaxed criteria. The advantage of using SNO events for intercalibration is that it allows for significant reduction of uncertainties owing to time and location mismatches in the comparisons, thus revealing instrument performance characteristics such as radiometric biases. Although the SNO method has been used widely for nadir-viewing passive radiometers, its application to radio occultation is fairly new and novel because we recently discovered that at the SNO between two RO LEO satellites, opportunities for simultaneous limb sounding also exist. In this case, the two LEO satellites at the SNO have simultaneous radio occultations occurring at nearly the same time, within short distance, receiving the same GNSS signals from the same GNSS satellite traveling along nearly identical atmospheric path. Figure 1 illustrates such a scenario in which *MetOp-B* met COSMIC-2 Flight Module 3 (COSMIC-2-FM3

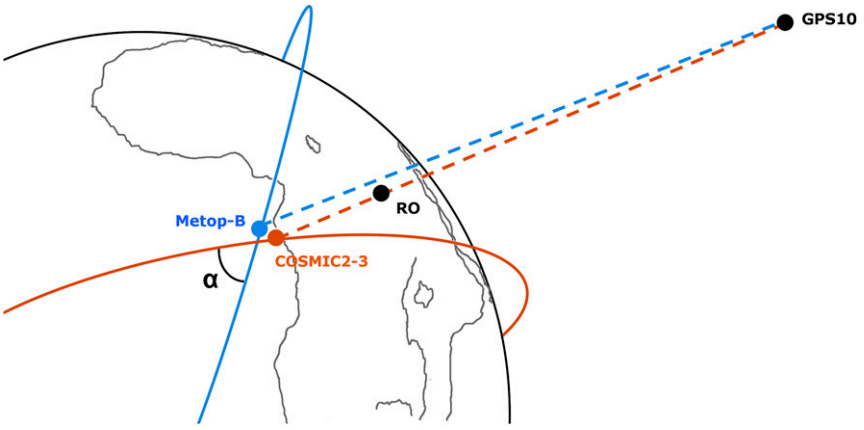

FIG. 1. Simultaneous radio occultation between *MetOp-B* and COSMIC-2-FM3 to GPS No. 10 (NAVSTAR_75_USA_265_41019) at 0903–0905 UTC 19 Oct (*MetOp-B* is setting while COSMIC-2-FM3 is rising).

hereinafter) at the SNO at 0903 UTC 19 October, at which both generated radio occultation measurements from GPS satellite No. 10. The entire event occurred within ~2 min, and the distances between the atmospheric profiles are as small as 15 km at an altitude of 10 km but still within 150-km distance for the entire event. This type of event creates good opportunities for bending angle intercomparisons between satellites for RO instrument and processing algorithm performance characterization.

In this particular case, *MetOp-B* was flying at a nominal altitude of 830 km while COSMIC-2-FM3 was flying at ~720-km altitude, which is lower than that of *MetOp-B* by about 110 km. Given the formula of SNO, we estimate that the SNO events occur about once every 2–3 days, although simultaneous RO events may not necessarily occur for each SNO event from both satellites. Similarly, SNOs exist between COSMIC-2-FM1 and other COSMIC-2 satellites for the period of this study, since COSMIC-2-FM1 had been lowered to the 550-km final orbit while the other five satellites remained in 720-km orbits, all with orbital inclination angles of approximately 24°.

Although it is true that in the final orbital configuration, the goal of COSMIC-2 is to have all six satellites in the ~550-km-altitude orbit, and therefore there will be no SNOs once orbital phasing is completed approximately 18 months after launch. However, the RO@SNO study is applicable before the final orbital configuration is in place. On the other hand, the method is not limited to the COSMIC-2 constellation. In addition to the *MetOp-B* case discussed earlier, there are many other missions including *KOMPSAT-5*, *Paz*, COSMIC-1, and smallsat RO receivers on polar-orbiting satellites, for which the method would be readily applicable.

Here, we introduce three angles to facilitate the discussion. One is the SNO α angle, which is the smaller angle at the SNO orbital intersection (Fig. 1). This angle is determined by the inclination and right ascension of ascending node (RAAN) angles of the two LEO satellites and is given by

$$\alpha = \cos^{-1}[\sin(i_1)\sin(i_2)\cos(\Omega_1 - \Omega_2) + \cos(i_1)\cos(i_2)], \quad (1)$$

where α is the SNO α angle; i_1 and i_2 are the inclination angles of satellite 1 and 2, respectively; and Ω_1 and Ω_2 are the RAANs of the two LEO satellites. Note that because the SNO α angle is defined to be the smaller angle at the SNO intersection, if $\alpha > 90$ then $\alpha = 180 - \alpha$.

The second angle is the RO@SNO θ angle, which is the angle between the two occultation planes. In this study, we assume the occultation planes are flat for simplicity. At the exact SNO point, θ is zero, but it increases as a function of the distance between the two LEO satellites away from the SNO intersection point, and in turn is determined by the SNO time difference between the two satellites, as well as the α angle. When θ is 0, it means that the occultations from each of the two LEO satellites are on the same occultation plane, which is an ideal condition for comparison. However, this rarely is the case, and a typical scenario is that they each pass the SNO orbital intersection point minutes apart.

For the RO@SNO events, the smaller the θ angle, the more ideal the intercomparison of bending angles is. The θ angle is partially determined by the α angle, assuming all other conditions are the same. For example, in the COSMIC-2 case, the SNO α angle is ~12.94° between satellite COSMIC-2-FM1 and COSMIC-2-FM4. This is in contrast to the SNO α angle of 59.96° between *MetOp-B* and COSMIC-2-FM3 (with inclination angles of ~98° versus 24°, respectively). As a result, there are more bending angle profiles meeting the SNO criteria for within COSMIC-2 satellites, than between *MetOp-B* and COSMIC-2 satellites.

The third angle involved in this study is the azimuth angle, which is defined here as the angle between the satellite velocity vector and the vector from the LEO to the GNSS satellite [similar to definitions in Schreiner et al. (2011) and Foelsche et al. (2011)]. Although this angle may affect certain performance parameters of the receiver, such as signal to noise at high angles (such as >50°), it generally is not a major factor affecting the comparisons in this study and therefore is not elaborated here except in anomalous cases where this angle is also large.

The procedure for predicting RO@SNO events are outlined here. First, an SNO between two LEO satellites with GNSS

receivers can be predicted using the SGP4 orbital perturbation model with two-line elements as input (Cao et al. 2004). Then, a time window approximately ±5 min from the SNO intersection is used in predicting occultation events by searching for GNSS satellites within a range of azimuth and elevation angles. The tangent points to Earth for the line of sight from the LEO satellites to the same GNSS satellite can be found, and their latitude/longitude can be calculated. Last, the distance between the two tangent points for the two LEO satellites can be estimated. If it is within a threshold (such as 125 km), it is considered an RO@SNO event.

The RO@SNO is an analytical method based on the first principle of orbital dynamics and has predictive capabilities that are beyond the capability of traditional collocation method. Since such events occur infrequently, the analyst only needs to get the data at the predicted time (typically for a few minutes of data) that are only a very small fraction of the total data volume, leading to significant savings in computing, processing time, and resources, with greatly reduced uncertainties in the analysis. It also allows us to perform in-depth diagnostic analysis of various parameters in the processing for individual cases of RO events that can lead to significant improvements in the processing algorithms and data quality.

3. Datasets and analysis procedure

To demonstrate the usefulness of the RO@SNO method, we defined a study period of approximately five months from 1 October 2019 to 16 February 2020, corresponding to the time period of COSMIC-2 provisional release data, while at the same time *KOMPSAT-5* and *Paz* data are also relatively stable. Two types of datasets and analysis are identified: one is data comparisons between the six COSMIC-2 satellites; the other consists of coincidental RO measurements between COSMIC-2 and other missions including *MetOp-A*, *MetOp-B*, *MetOp-C*, COSMIC-1, *KOMPSAT-5*, and *Paz*.

a. COSMIC-2 TGRS dataset

The six COSMIC-2 satellites were successfully launched on 25 June 2019. COSMIC-2 is the follow-on mission of COSMIC-1 that was launched in June 2006 and successfully demonstrated the feasibility of RO data for climate, weather, and space weather applications (Ho et al. 2020). After an extensive calibration/validation period, the first COSMIC-2 provisional dataset was released on 11 December 2019 by the COSMIC-2 team (Weiss 2019). According to the release note, the FORMOSAT-7/COSMIC-2 satellites were launched into a 24° inclination low-Earth orbit. Following spacecraft system activation and checkout, instruments were first activated on 16 July 2019. The main interest for this release was in the TGRS payload, for which the data release includes the neutral atmosphere products from 1 October 2019 and forward.

Three levels of data products are included in the release, each corresponding to steps in the radio occultation processing chain: 1) level-0 raw TGRS binary data files; 2) level-1a precise orbit determination antenna measurements (RINEX v2 format), satellite attitude measurements (leoAtt format), high-rate RO measurements (opnGns format) and level-1b precise orbit determination solutions (SP3 format), atmospheric excess phase (conPhs format); and 3) level-2 atmospheric profiles as atmPrf (RO retrieval), wetPf2 (1D-var retrieval), as well as level-2 data in BUFR format. In this study, we mainly used the bending angle and dry atmospheric profile data that are in the level-2 products, as well as signal-to-noise ratio and timing information that is in the lower-level products.

As discussed earlier, there is a trade-off between the number of samples and the RO@SNO criteria. Among the six COSMIC-2 satellites, we found 504 cases (including 398 for GPS and 106 for GLONASS) that met the criteria of 10-min separation in time and 125 km in distance. However, based on the quality flags in the data, 441 cases are of good quality. As a result, 63 bad cases are excluded in the subsequent analysis.

b. MetOp-A/B/C *GRAS RO@SNO with COSMIC-2 TGRS dataset*

MetOp-A/*B*/*C* were launched into the midmorning orbit in the same orbital plane on 19 October 2006, 17 September 2012, and 7 November 2018, respectively. Among the instruments on *MetOp-A*/*B*/*C*, GRAS is a GPS receiver that provides radio occultation capabilities. The MetOp satellites fly at a nominal altitude of 830 km, which is about 110 km above the 720-km altitude orbit where from three to five of the six COSMIC-2 were located during the period of this study. The orbital altitude differences create opportunities for SNO as discussed earlier. On the other hand, the MetOp satellites are in a polar orbit while COSMIC-2 is in a low inclination orbit. The inclination angles are 98° for MetOp and 24° for COSMIC-2. As a result, the RO@SNO occultations from the same GNSS satellite have very different azimuth angles relative to the satellite velocity vectors of MetOp and COSMIC-2. This is not a major problem because the GNSS receivers have a large ''field of view,'' approximately half dome, although this does lead to rapid increase in distance separation away from the SNOs. Nevertheless, RO@SNOs can be found between MetOp and COSMIC-2. In this study, totals of 136, 98, and 104 matchups between COSMIC-2 and *MetOp-A*/*B*/*C*, respectively, meet the same criteria of 10 min and 125 km in distance after excluding bad-quality cases. They are used to demonstrate the concept of this method for the period of study.

After the data are selected, the following procedure is used in analyzing the data:

1) As an option, the scenario can be simulated using the Satellite Tool Kit (STK) to verify the RO@SNO event for intuitive visual verification. This is done by creating a scenario in STK and adding the two LEO satellites involved, as well as the GNSS satellite. Note that in the STK database there may be multiple GNSS satellites labeled as having the same pseudorandom noise sequence (PRN) number, possibly due to reassignment over time, but in reality a PRN is unique at any given time for identifying each satellite in the active constellation. Therefore, only the one with ''operational'' status should be used. The time window of the event is specified, and an ''access'' analysis is performed from each LEO satellite to the GNSS satellite. This generates a 3D graphic display of the event that

confirms the validity of the event for the analysis. This step is only necessary for visually verifying the RO@SNO events.
2) The bending angle profiles are extracted from the data produced by the two satellites, and the ratio as well as differences between the bending angles are plotted as a function of altitude.
3) The distance as a function of altitude is plotted to assess the spatial separation of the two profiles.
4) The dry temperature profiles and their differences, as well as graphic plots of other parameters are made to assist the analysis.

Note that, for a given RO@SNO event, the criterion of 125 km in distance may not be met for a given bending angle profile at all altitudes, especially for MetOp and COSMIC-2 matchups where the distance is rapidly growing with time because of large α angles. In such cases, only the portion of the bending angle that met the criteria is included in the statistical analysis.

c. *COSMIC-1,* KOMPSAT-5*, and* Paz *IGOR versus COSMIC-2 TGRS*

After ~14 years of successful operations, the COSMIC-1 satellite constellation has degraded to a point where there was only one satellite (COSMIC-1-FM6) producing data for a portion of the study period. There was a significant decrease in the number of occultations per day after October 2019 that greatly reduced the number of cases in this study. As a result, only four good cases are found between COSMIC-1 and COSMIC-2 for the study period. Nevertheless, we found that the comparisons are informative as discussed later.

KOMPSAT-5 is a low-Earth-orbiting satellite mission that includes a primary synthetic aperture radar (SAR) payload and a secondary atmospheric radio occultation payload, the Atmosphere Occultation and Precision Orbit Determination (AOPOD) instrument. A collaboration between the United States and South Korea enables *KOMPSAT-5* RO data to be operationally downlinked via NOAA's Fairbanks, Alaska, ground station, and in turn, NOAA has near-real-time access to the *KOMPSAT-5* RO data for numerical weather prediction. The *KOMPSAT-5* satellite has an inclination angle of 97.6° and nominal altitude of 550 km. The RO capability of *KOMPSAT-5* includes the IGOR receiver, which is the same type of receiver flown on COSMIC-1 and other missions. For the period of study, we found 36 good-quality cases that met the study criteria after excluding 42 cases that were flagged as bad quality indicated in the metadata. Note that all *KOMPSAT-5* rising occultations are flagged as bad. The distances between the RO profiles are typically in the range of 8–33 km for the selected samples between COSMIC-2 and *KOMPSAT-5*.

The *Paz* satellite is a Spanish low-Earth-orbiting satellite mission that includes a GPS RO payload. *Paz* was launched on 22 February 2018, with a secondary payload of Radio Occultation and Heavy Precipitation with *Paz* (ROHPP). The ROHPP instrument makes use of the original IGOR+ receiver but with a distinct capability of polarimetric RO—a proof-of-concept experiment for the detection of heavy precipitation. This is the first time that polarimetric GPS signals are captured from space, and the first attempt to monitor precipitation by means of RO techniques. Through collaboration between the United States and Spain, NOAA provides remote tracking stations downlink via the Fairbanks Command and Data Acquisition Station. NOAA has near-real-time access to the data for weather applications. Similar to *KOMPSAT-5*, *Paz* produces on the order of 200 ROs per day. For the study period, we found 30 *Paz* cases meeting the study criteria, after excluding 11 cases that were flagged as bad in the data stream.

4. Results and discussion

In this section, we first analyze a *MetOp-B*/COSMIC-2 sample RO@SNO case to introduce the method for several reasons: 1) *MetOp-B* and COSMIC-2 are two different RO systems developed by different countries with different GNSS receivers. 2) *MetOp-B* is in a midmorning polar orbit, while COSMIC-2 is in a low inclination orbit. Given the large inclination angle differences, it is a more challenging scenario for comparisons, which can provide illuminating results from using this method. 3) Each system is known to have its own performance characteristics. We are interested in verifying these known characteristics. Following the *MetOp-B* sample, we further analyzed cases with *MetOp-A*/*B*/*C*, COSMIC-1, *KOMPSAT-5*, and *Paz*. While the GRAS on MetOp is very different from the TGRS receiver, the IGOR receiver on *KOMPSAT-5* and *Paz* have the heritage of COSMIC-1. After the MetOp, COSMIC-1, *KOMPSAT-5* and *Paz* analysis, we will examine the case between pairs of the COSMIC-2 satellites. Since in the latter case all satellites have smaller SNO α angles, and have the same type of receivers, it becomes relatively straight forward as we demonstrate later. We point out that MetOp RO can be best used as a reference for polar-orbiting satellites, including a large constellation of commercial satellites since many have similar inclination angles. On the other hand, COSMIC-2 can be best used as reference for low inclination satellites, especially after completing the orbital phasing. Note also that, although the sample size is limited, we expect that such events will increase over time from several factors, including the expansion to other GNSS systems for RO such as GLONASS, Galileo, Bai Dou, QZSS, and others. With more modern receivers that can take advantage of all GNSS systems, and the fact that the RO constellations will continue to increase in the foreseeable future, the RO@SNO method will become more useful.

a. *RO@SNO between MetOp and COSMIC-2*

A sample case of a *MetOp-B* versus COSMIC-2-FM3 RO@SNO event occurred at 0903–0905 UTC 19 October (Day 292) 2019. In this event, both RO instruments on *MetOp-B* and COSMIC-2-FM3 were receiving signals from GPS No. 10 (NAVSTAR75). The SNO event occurred near the coast of Africa, although the occultation occurred over Central African Republic (7.5710°N, 24.4710°E) near the border with South Sudan (Fig. 1) during the hot and dry season. For this event, *MetOp-B* had a setting occultation, while COSMIC-2-FM3 had a rising occultation. The separation between the two profiles varies with altitude, but at all altitudes the distance between them is within 150 km. At the closest distance, which

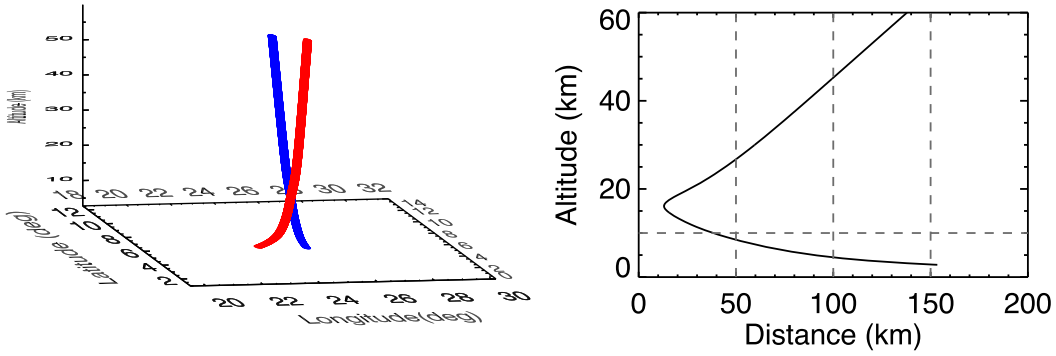

FIG. 2. Distance as a function of altitude for the *MetOp-B*/COSMIC-2-FM3 RO@SNO event (0903–0905 UTC 19 Oct 2019): (left) the three-dimensional geolocation of the two occultations and (right) the separation between the two profiles with altitude.

is at about 15-km altitude, the separation is less than 15 km. The time difference is within 1 min 46 s. Although this criterion is still more relaxed relative to the traditional SNO standards, it is again more stringent relative to the typical comparisons for radio occultation data that generally consider collocations within 250–300 km in distance and 3-h difference in time. The right panel of Fig. 2 shows the distance between the two retrieved profiles at altitudes from the ground to 60 km above mean sea level. The horizontal dashed line indicates 10 km in altitude. The left panel of Fig. 2 illustrates the exact location of the occultation path during the event. Note that the two occultations diverge from one another both above and below the point of closest approach at 17.5-km altitude.

Given the time difference of ~2 min, we assume that the atmospheric temperature and water vapor have not changed significantly during this event. This assumption is generally valid, perhaps with exceptions during severe weather events. The other important assumption is that the atmosphere is horizontally uniform within the area of observation. We acknowledge that this assumption may not be always valid for all layers of the atmosphere, since the distance between the two measurements varies depending on the altitude. In general, we believe that the shorter the distance is, the more uniform it is in the atmosphere between the two points of measurements. Typically, the smaller the distance is, the better it meets this assumption. This is consistent with the spherical symmetry assumption (or absence of horizontal gradients) as discussed in Kursinski et al. (1997). It is known that this assumption contributes to uncertainties of RO data in the stratosphere and upper troposphere. In the lower troposphere, horizontal gradients may cause impact parameter multipath, invalidating the retrieval assumptions and thus introducing bias in the bending angle. As a result, our method proposed in this study does not make a more stringent assumption on the horizontal structure of the atmosphere than the retrieval does, and is consistent with the physics of the retrieval.

The left panel of Fig. 3 shows that the bending angle difference, expressed as a ratio between the two (COSMIC-2-FM3/*MetOp-B*),

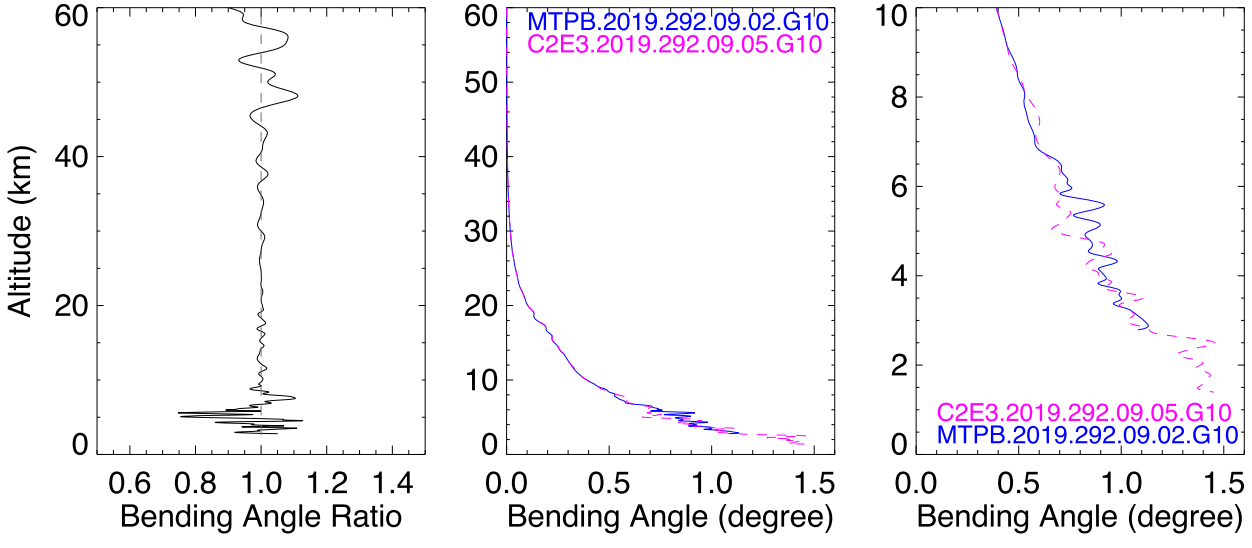

FIG. 3. Bending angle for the *MetOp-B*/COSMIC-2-FM3 RO@SNO event: (left) bending angle ratio, (center) *MetOp-B* and COSMIC-2 bending angle comparison, and (right) bending angle comparison zoom-in for <10-km altitudes.

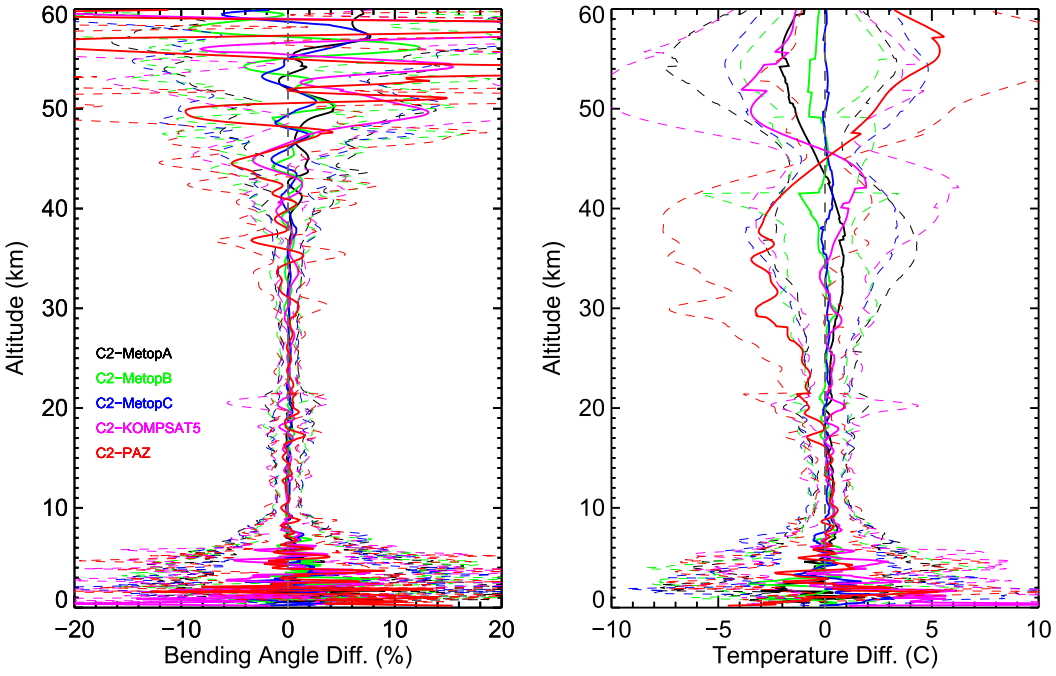

FIG. 4. RO@SNO comparison between COSMIC-2 (C2) and *MetOp-A*/*B*/*C*, *KOMPSAT-5*, *Paz* from 1 Oct 2019 to 16 Feb 2020 [criteria: 10 min, 125-km differences; (left) bending angle; (right) dry temperature]; solid lines indicate bending angle ratio, and dashed lines indicate standard deviation.

and the center panel of Fig. 3 compares the actual bending angles. It can be seen that three segments can be identified by altitude: between 8 and 45 km, the bending angle differences are small (<3%). The best agreement is achieved at ~25-km altitude (<1%). For altitudes above 45 km, the bending angle differences can be up to 15%. This is partly due to the fact that the bending angle becomes extremely small. For altitudes below ~8 km, the bending angle differences between *MetOp-B* and COSMIC-2-FM3 are relatively large, up to 25% for individual points (a ratio as low as 0.75 at ~5-km altitude). The large differences below 8 km can be due to several factors, including the increased nonuniformity of the atmosphere horizontally and a known issue with *MetOp-B*/GRAS open-loop tracking approach that relies on feedback from a delay-locked loop (Schreiner et al. 2011). The right panel of Fig. 3 is a zoom-in on this RO@SNO case below 10 km in altitude. It shows that our method is able to reveal the detailed bending angle characteristics for COSMIC-2-FM3 and *MetOp-B* due to both instrument and processing algorithms down to near the surface, which would greatly benefit the calibration/validation for the RO missions involved.

Statistical analysis for similar cases during the study period for other radio occultation missions are also performed. Figure 4 and Table 1 show results from the statistical analysis of the COSMIC-2 versus *MetOp-A*/*B*/*C*, COSMIC-1, *KOMPSAT-5*, and *Paz* cases for the study period from 1 October 2019 to 16 February 2020. Figure 4 (left panel) shows the bending angle differences, while Fig. 4 (right panel) shows the dry temperature differences. Several characteristics are found:

1) Among the comparisons between the three MetOp instruments and COSMIC-2, the best agreement is found between *MetOp-C* (blue curve) and COSMIC-2 from about 8 up to 60 km. *MetOp-B* (green curve) also agreed with COSMIC-2 well, although differences are found at >35-km altitude. In contrast, *MetOp-A* (black curve) has relatively large biases when compared with COSMIC-2 at altitudes > 30 km. Although the root cause for the differences between *MetOp-A*/*B*/*C* is not known and requires further investigation, *MetOp-C* is the latest in the MetOp series and possibly have incorporated the latest improvements, while *MetOp-A* has degraded and is being phased out of the orbital plane.
2) Despite the small number of samples, very good agreement is also found between COSMIC-2 and COSMIC-1. Figure 5 shows the bending angle differences between COSMIC-1 and COSMIC-2 for the four good cases, as well as their averages.
3) Comparison between *KOMPSAT-5* and COSMIC-2 shows good agreement at altitudes below 35 km, but differences increase at higher altitudes (Fig. 4). Larger differences are found between *Paz* and COSMIC-2 starting from 20 km toward higher altitudes. We have tested several ideas to reduce this bias, such as excluding COSMIC-2 L2P rising cases, and excluding low SNR for both COSMIC-2 and *Paz* cases (some had high azimuth angles). While the bias can be reduced slightly, none of them removed the bias pattern entirely and this bias appears to be systematic. Analysis does not show significant correlation between SNR at high altitude and the bias. A similar bias was shown in a previous

TABLE 1. Bending angle comparison (% difference) between COSMIC-2 and *MetOp-A*/*B*/*C*, COSMIC-1, *KOMPSAT-5*, and *Paz* (the three numbers in each altitude bin represent the bias, standard deviation, and number of cases).

Altitude	C2/*MetOp-A*	C2/*MetOp-B*	C2/*MetOp-C*	C2/*KOMPSAT-5*	C2/*Paz*	C2/C1	C2-FM/C2
40–60 km	2.25	0.49	0.58	5.22	2.65	−3.15	1.76
	9.40	10.26	9.69	18.83	28.08	5.28	45.23
	47	22	40	11	7	2	282
30–40 km	0.13	0.00	0.18	0.21	−0.53	−0.39	−0.05
	1.31	1.53	1.47	1.42	2.51	1.68	1.95
	68	34	51	14	7	2	321
20–30 km	0.13	0.10	0.10	0.03	0.28	0.18	−0.01
	1.09	1.00	0.86	1.17	1.13	0.95	1.64
	93	52	69	19	13	4	368
10–20 km	−0.01	0.11	0.09	−0.03	0.07	−0.07	0.00
	1.40	1.51	1.42	1.44	1.23	1.18	1.31
	128	93	94	32	27	4	426
5–10 km	0.14	0.10	0.40	0.21	0.42	0.81	0.10
	4.41	4.18	4.47	4.83	4.13	5.45	5.03
	122	93	94	31	28	4	424
0–5 km	2.20	1.61	0.39	−2.45	2.60	5.83	1.21
	11.02	10.46	10.73	12.53	10.50	11.78	14.59
	71	57	51	24	19	3	362

study when comparing *Paz* with ECMWF where the bias increases from 30 to 40 km in *Paz* (Hunt et al. 2019). The temperature bias can be traced back to a bias in bending angle, and in turn to excess phase in the data processing. *Paz* RO processing is different from other missions since it combines horizontally and vertically polarized signals to produce the excess phase (Hunt et al. 2019). There are several possible factors that can introduce uncertainties in the excess phase in the close loop stage (typically >20 km) where the large relative bias in *Paz* presents, such as residual uncertainties in the L2 phase smoothing and extrapolation before bending angle conversion, residual clock error, and quality control criteria used. Several *Paz* profiles indicated as ''good'' in the data stream appear to be out of range in dry temperature (>10 K) with large variations above 30 km relative to COSMIC-2. A stricter quality control for the *Paz* dataset are likely needed for users. The root cause of this bias requires in-depth analysis of the data

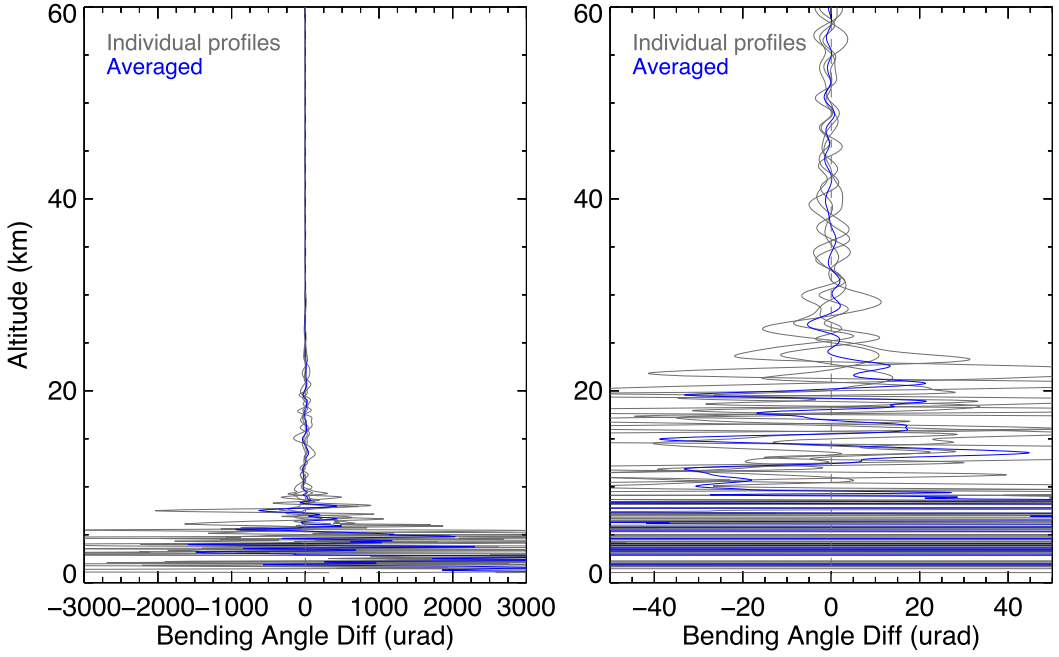

FIG. 5. (left) COSMIC-1 and COSMIC-2 bending angle comparisons (gray = individual profiles; blue = averaged profile). (right) The same comparison but with a different range on the horizontal axis.

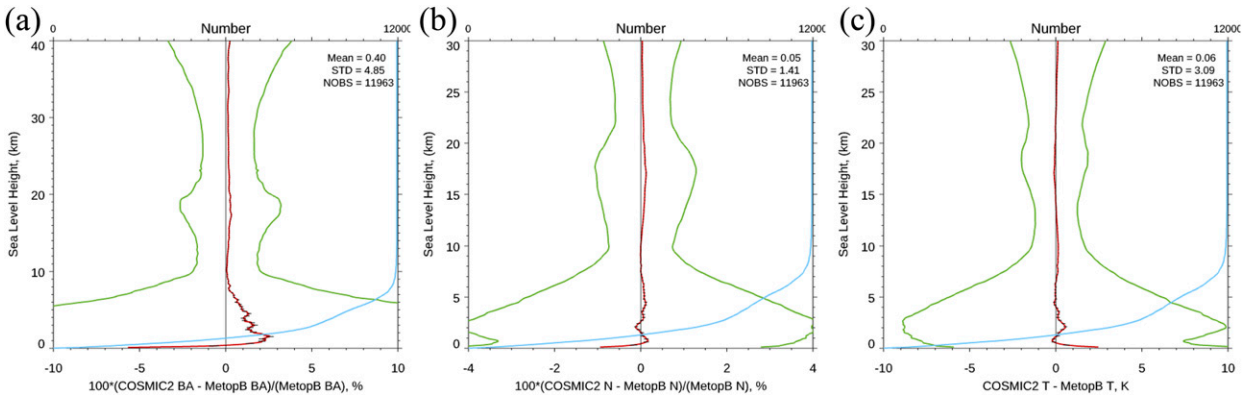

FIG. 6. Independent statistical analysis and validation of the *MetOp-B* vs COSMIC-2 collected from 1 Oct 2019 to 16 Feb 2020 (COSMIC-2 and *MetOp-B* within a 2-h time window and 300-km distance window): (a) bending angle, (b) refractivity, and (c) dry temperature.

processing, and we plan to work with the data processing center at UCAR to further investigate in the near future.

4) Figure 4 (right panel) shows that below 8 km the differences in the dry temperature profiles between COSMIC-2 and other missions can be large. This can be due to several factors. The first factor is potential nonuniformity in the atmosphere since the distance between the profiles can be up to 125 km. It is known that the troposphere layers are less uniform horizontally compared to the upper atmosphere. Differences could also be due to instrument performance or processing algorithms, such as the handling of multipath effects or signal to noise ratio differences, as discussed in the *MetOp-B*/GRAS case earlier. The temperature differences above 40 km are likely due to the very small values in the bending angles, and the fact that further optimization is also needed for COSMIC-2 retrievals.

In the comparisons above, both bending angle and dry temperature differences are analyzed as shown in Fig. 4. Bending angle is a key product parameter for GNSS radio occultation for several reasons: 1) bending angles are calculated based on excess phase, which is based on direct measurement of GNSS signal time delay due to atmospheric effects. 2) Bending angles are the key parameter used in direct assimilation into numerical weather prediction models. 3) Uncertainties in calculating bending angles are reduced to a minimum because the calculation does not rely on complex models and associated uncertainties. Therefore, the comparison of bending angles, whenever possible and properly designed, should have minimal uncertainties.

It is also useful to compare the retrieved atmospheric profiles that can be readily interpreted by meteorologists and Earth scientists. In this study, we only compare the ''dry temperature profiles'' that are directly retrieved from bending angles with the assumption that there is no moisture in the atmosphere. The ''wet temperature profiles'' additionally rely on weather models such as ECMWF as well as associated uncertainties from 1D-var retrieval. In general, as the retrieved product level increases from level 1 to 2 and beyond, the uncertainties grow significantly in comparisons, and as a result, it becomes difficult to separate instrument performance from model uncertainties.

Further comparisons between MetOp and COSMIC-2 are performed with results from an alternative method for cross-check, where the matching criteria are within 2 h in time and the distance window is within 300 km. The result is in general agreement with the RO@SNO method, which also suggests that there is a relatively large difference in the bending angle (up to ~2.5%), refractivity, and dry temperature, from COSMIC2 and those from *MetOp-B* with larger standard deviations, at altitudes below 8 km (Figs. 6a–c).

b. *RO@SNO between COSMIC-2 satellites*

Note that the COSMIC-2 satellite orbits are changing during the orbital phasing period that takes approximately 18 months after launch. The final orbital configuration is then achieved after orbital phasing. Shortly after launch, the six COSMIC-2 satellites were in the same orbital plane, following each other closely in a constellation similar to the NASA ''A''-Train satellite constellation configuration. During this time, opportunities existed to perform coplanar comparisons between satellites as discussed in section 1. However, the distance between pairs of the six satellites grows over time. In addition, orbital phasing maneuvers are performed to lower the satellites to 550-km altitude in six different orbital planes with 60° separations in RAAN. For the study period, the COSMIC-2-FM1 satellite was first lowered successfully into the 550-km orbit, while the rest of the satellites were gradually lowered from their initial 720-km altitude. Given the principles of SNO as discussed earlier, the orbital altitude differences lead to SNO events. Furthermore, unlike the RO@SNO with MetOp, the SNO α angles between COSMIC-2 satellites are smaller. Figure 7 illustrates a RO@SNO event between COSMIC-2-FM1 and COSMIC-2-FM4, where both TGRS receivers were rising and receiving occultation signals from GPS No. 3 over the Pacific Ocean at night within 4 min 33 s. Similar to the analysis for *MetOp-B*, here we present results for COSMIC-2 samples.

The right panel of Fig. 8 shows that the distance between these two RO profiles is within 58 km at all altitudes and within 32 km at 5-km altitude. The left panel of Fig. 8 shows that these two profiles are relatively close to each other at all altitudes

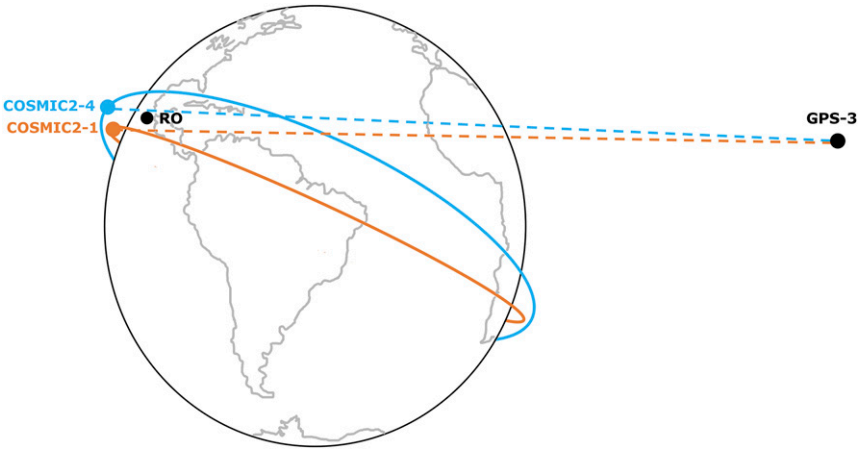

FIG. 7. RO@SNO between COSMIC-2-FM1 and COSMIC-2-FM4 (0929–0934 UTC 1 Oct 2019).

because of the smaller RO@SNO α and θ angles between the two COSMIC-2 satellites. This is in contrast to the previous case for *MetOp-B* where the divergence in distance can be significant between *MetOp-B* and COSMIC-2 at different altitudes.

Statistical results using the 441 COSMIC-2 RO@SNO cases are presented in Fig. 9, which shows several characteristics: 1) Excellent agreement between COSMIC-2-FM1 and other COSMIC-2 satellites are found between ~8 and 40 km. Below 8 km, the data become noisy as expected, while above 40 km, uncertainties increase significantly due to the effect of instrument noise, GNSS clock errors, and ionospheric residuals on the small bending angles resulting from the tenuous atmosphere in the upper stratosphere (Kursinski et al. 1997; Ao et al. 2012; Schreiner et al. 2020). This is because although these errors remain largely the same with height throughout the atmospheric vertical profile, as the bending angle decreases exponentially with increasing height, the relative effect of these errors becomes large, while in the lower atmosphere, other sources of error dominate. Below 8 km, the result suggests that the measurements are more consistent between the COSMIC-2 satellites (<5%), than with MetOp (shown in Fig. 4) that has larger spread in the differences (up to ~8%). 2) The standard deviation below 8 km is large (up to 20%, comparable to the MetOp case), while the standard deviation is smaller between 8 and 30 km in altitude except for an increase around 20 km, likely due to a known L2P tracking issue, particularly for rising occultations, which will be discussed later.

Overall, the agreement between COSMIC-2 RO profiles are better than those with MetOp, especially below 10 km. It is possible that the TGRS outperforms the GRAS on *MetOp-B* at low altitudes since both the COSMIC-2 and *MetOp-B* datasets are produced by UCAR with similar processing algorithms to retrieve the bending angle from excess phase measurements. However, the larger uncertainties in the comparison between COSMIC-2 and MetOp may be due to the large SNO α and θ angles and the greater distance between the profiles. The results presented here are very consistent with the coplanar COSMIC-2 comparison (Schreiner et al. 2020; Ho et al. 2020, manuscript submitted to Remote Sens.).

The anomalous feature seen at ~20 km in Fig. 9 requires further investigation. Here we use a selected case for more detailed analysis. Figure 10 (curve in the foreground) shows an RO@SNO event between COSMIC-2-FM1 and COSMIC-2-FM2 at 1421 UTC day 341 for GPS No. 11, which indicates a bending angle anomaly at 20-km altitude (about 8% difference).

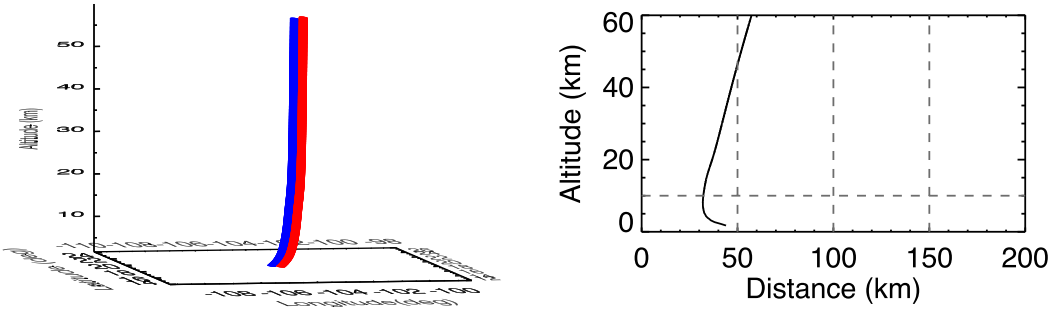

FIG. 8. RO@SNO event between COSMIC-2-FM1 and COSMIC-2-FM4 on day 274 (1 Oct 2019) at 0931 to 0934 UTC: (left) the three-dimensional geolocation of the two occultations and (right) the separation between the two profiles with altitude.

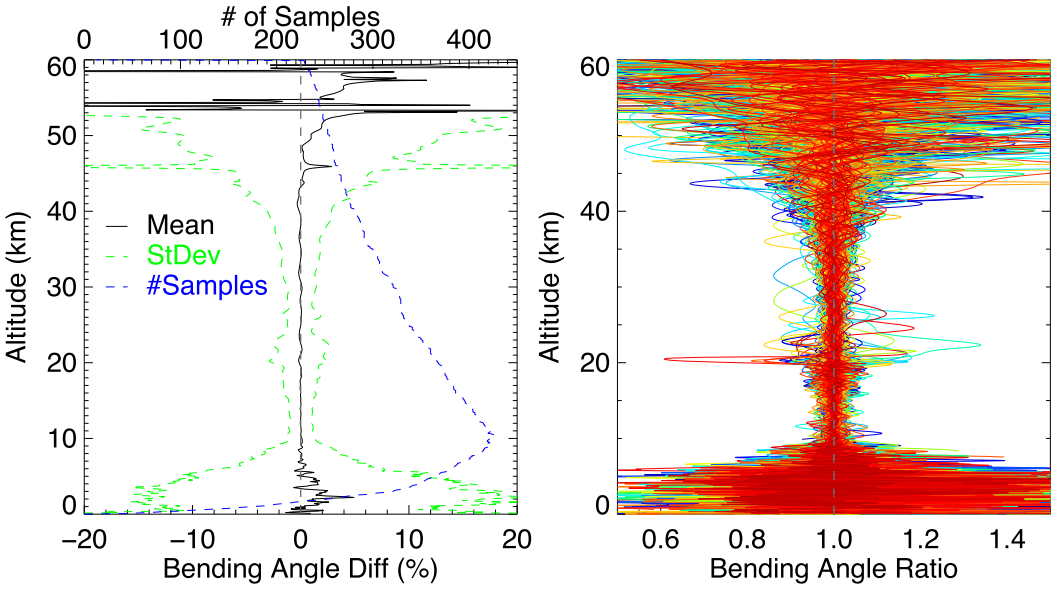

FIG. 9. Bending angle difference for the RO@SNO between COSMIC-2-FM1 and the other five COSMIC-2 satellites. (left) The average bending angle ratio is shown by the black solid curve, and the standard deviation is shown by the dashed green curve; also shown is the number of samples vs altitude (blue dashed curve). (right) The bending angle ratio for all cases, shown with curves of various colors.

This anomaly led to large departures in the retrieved temperature profile (Fig. 10, right panel). Analysis shows that the distance between the two is within 20 km at this altitude and the time difference is within 3 min. This would be a good scenario for bending angle comparisons so the large difference in bending angle could not be easily explained. A closer examination of the provisional release memo suggests that this is a COSMIC-2 L2P rising case that is a known problem to the COSMIC-2 program, and the retrieved profile may have large errors. According to the release memo (Weiss 2019),

> GPS L2P rising occultation bias and standard deviation are higher than setting occultations from approximately 19–29 km altitude. The TGRS v4.3.2 flight software reduced but

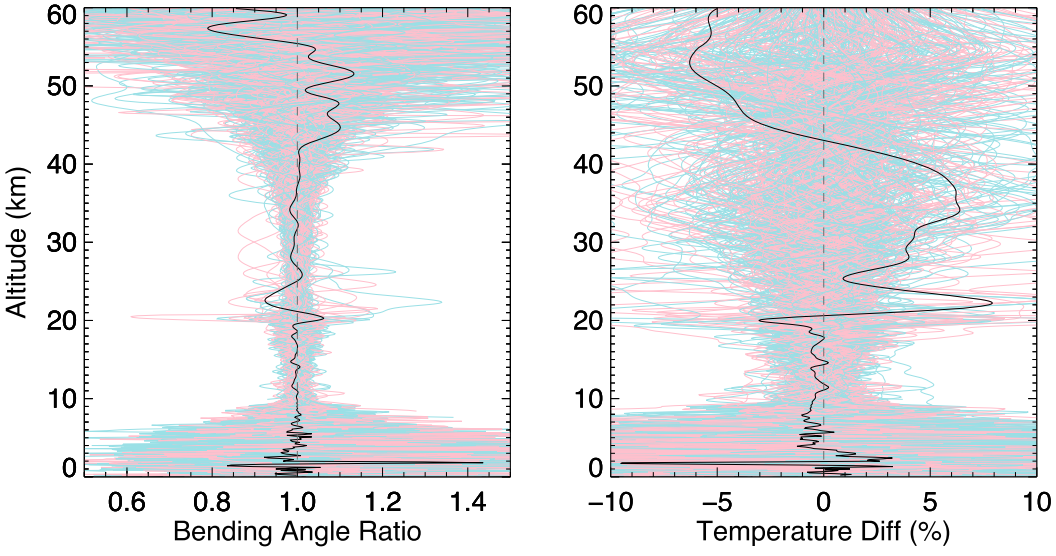

FIG. 10. (left) Bending angle ratios and (right) temperature differences for COSMIC-2-FM1 and the other COSMIC-2 satellites. Setting occultations are indicated by blue curves, and rising occultations are given by red curves. The black curve in the foreground represents the selected example case discussed in the text. Anomalies due to the L2P tracking issue can be seen at 20 km in the selected case as well as in a number of rising and setting cases.

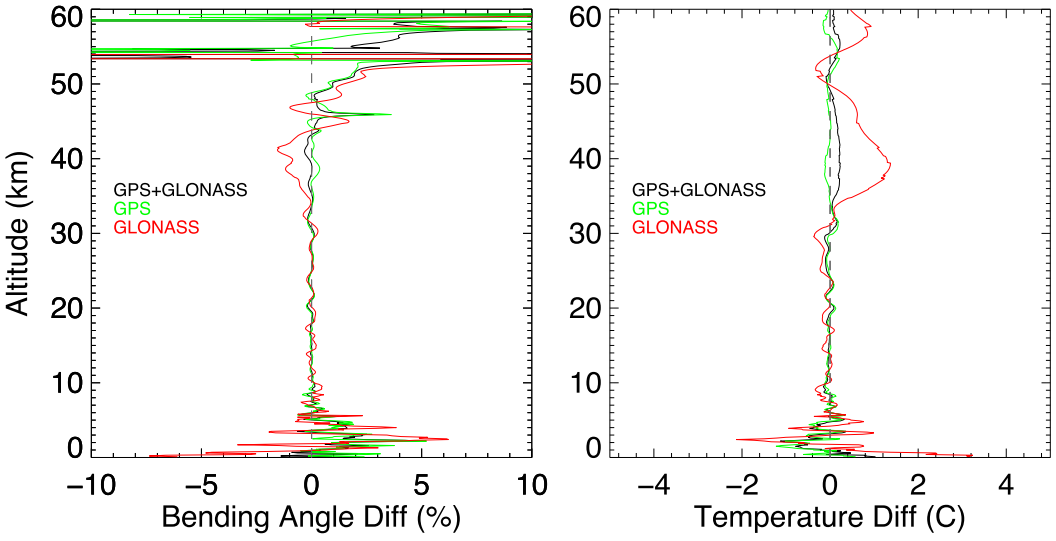

FIG. 11. (left) The average percent difference in bending angles and (right) average temperature differences between COSMIC-2-FM1 and the other COSMIC-2 satellites for GPS (green curves), GLONASS (red curves), and all occultations (black curves).

did not eliminate this feature, and the team continues to investigate. . . . On the date of this memo, the affected GPS PRNs are 2, 4, 11, 13, 14, 16, 18, 19, 20, 21, 22, 23, 28.

The L2P anomaly affects ~10% of profiles on average. The errors arise in the region where the transition between applying the standard ionospheric correction that requires that the L1 and L2 GPS signals be tracked simultaneously and an extrapolated correction occurs. The processing for the provisional dataset places this transition point at 20 km. However, for some L2P occultations with low SNR, the tracking for the L2 signal drops off above 20 km, thus the extrapolated ionospheric correction should begin at a higher altitude (Sokolovskiy et al. 2014). It should be noted that although the memo suggests that it affects only "rising" cases, in reality it affects "setting" occultations as well but in fewer cases because more rising occultations suffer from low SNR. The curves in the background of Fig. 10 shows all COSMIC-2 RO@SNO cases separated by rising (red) and setting (blue). It is observed that at ~20–25 km there are indeed anomalous cases in both rising and setting scenarios.

It is known that the TGRS on COSMIC-2 currently receives RO signals from both GPS and GLONASS satellites. A question often asked is whether radio occultation for these two systems could be different. Note that currently not all RO receivers can receive GLONASS signals but COSMIC-2, as a TriGNSS receiver, is among the first to be able to do so. To answer this question, in this study, we additionally separated all COSMIC-2 RO@SNO cases into GPS versus GLONASS to analyze their bending angle differences. Figure 11 (left panel) shows that bending angles from both GPS and GLONASS agree very well between altitudes 8 and 35 km. However, bending angles from GLONASS begin to deviate from those from GPS at higher altitudes and reached a maximum around 40 km. It is known that beyond 40 km, the bending angles become small and not as reliable, thus not typically assessed. In the low atmosphere (altitude below 8 km), the GLONASS cases appear to have a larger spread compared to those from the GPS. The deviations for GLONASS bending angles could be due to several factors, including the range of stability among the clocks on board various GLONASS satellites (Griggs et al. 2015). Fluctuations in GLONASS clock errors on time scales shorter than the frequency clock solutions used in processing introduce errors into the bending angle and retrieved variables, particularly at altitudes above 30 km. It is believed that some of these differences can be reduced in the near future by tuning the processing for GLONASS.

5. Conclusions

Previous GNSS RO intersatellite comparison studies relied on either global statistical comparisons with relaxed matchup criteria or coplanar analysis in early orbits that has a limited duration in time and is limited to multisatellite constellations. Our study demonstrates a new method of RO@SNO in which simultaneous radio occultation profiles can be compared near the orbital intersections of the two low-Earth-orbiting satellites, when receiving the GNSS RO signal from the same GNSS satellite passing through approximately the same atmosphere. The usefulness of this method has been demonstrated with comparisons between COSMIC-2 and *MetOp-A*/*B*/*C*, COSMIC-1, *KOMPSAT-5*, and *Paz*, as well as between the six satellites of the COSMIC-2 constellation. Instrument and processing algorithm performance characteristics are analyzed based on the bending angle and dry temperature differences.

For comparisons between COSMIC-2 and other missions, excellent agreement between COSMIC-2 and *MetOp-A*/*B*/*C*

GNSS RO bending angle profiles are found, especially at altitudes between 8 and 35 km. COSMIC-2 and COSMIC-1 bending angles also agreed very well although there are only very few cases available due to the degradation of COSMIC-1. Systematic biases in bending angle and dry temperature are found between COSMIC-2 and *Paz* in the mid- to upper atmosphere, as well as *KOMPSAT-5*, and determining the root causes will require further in-depth investigation working closely with the data processing centers.

Between COSMIC-2 satellites, the bending angle profiles agree very well for nearly all altitudes. However, bending angle profiles derived from GLONASS system appear to have larger uncertainties compared to their GPS counterparts at mid- to upper atmosphere. Anomalous bending angles are found near 20 km in altitude for COSMIC-2, known as the L2P rising issue, although such cases also exist in setting cases, leading to uncertainties in the retrieved dry temperature profiles as well. We plan to work closely with the COSMIC-2 data processing center at UCAR to further investigate all anomalies found in this study and to improve the quality of the data for users.

The RO@SNO method is believed to be a very useful complement to the traditional methods, especially for instrument and processing algorithm diagnostic purposes because it allows for in-depth analysis of individual RO events by examining all variables involved in the processing. Given the increasing number of GNSS RO constellations, both in the polar orbit and low inclination orbits for current and future missions, and the expansion of GNSS itself, we believe that this method will become increasingly useful for the calibration/validation of GNSS RO measurements and receiver performance evaluation going forward.

Acknowledgments. The authors thank Dr. Satya Kalluri and Dr. Yong Chen for a critical review of the paper with comments and suggestions. Thanks are extended to UCAR CDAAC for making all GNSS RO data available, including COSMIC-2, MetOp, COSMIC-1, *KOMPSAT-5*, and *Paz* data. We also thank Mr. Xinjia Zhou for developing and sustaining the GNSS RO Integrated Cal/Val System (ICVS) at the NOAA Center for Satellite Applications and Research, which has been used for validation of this study, as well as Dr. Xi Shao, for fruitful discussions on orbital perturbation and *Paz* antenna characteristics. This study is partially funded by the NOAA/NESDIS/OPPA Technology Maturation Project TMP-18-03 ''Accelerating the data assimilation of smallsats,'' and the COSMIC-2 calibration/validation program, with NOAA grant NA14NES4320003 [Cooperative Institute for Climate and Satellites (CICS)] to the University of Maryland/ESSIC. The article contents are solely the opinions of the author(s) and do not constitute a statement of policy, decision, or position on behalf of NOAA or the U.S. government.

Data availability statement. The MetOp, COSMIC-2, COSMIC-1, *KOMPSAT-5*, and *Paz* GNSS radio occultation data used for this study are available online (https://data.cosmic.ucar.edu/gnss-ro/cosmic2/provisional/ and https://cdaac-www.cosmic.ucar.edu/cdaac/products.html).

REFERENCES

Anthes, R. A., and Coauthors, 2008: The COSMIC/FORMOSAT-3 mission: Early results. *Bull. Amer. Meteor. Soc.*, **89**, 313–334, https://doi.org/10.1175/BAMS-89-3-313.

Ao, C., A. J. Mannucci, and E. R. Kursinski, 2012: Improving GPS radio occultation stratospheric refractivity retrievals for climate benchmarking. *Geophys. Res. Lett.*, **39**, L12701, https://doi.org/10.1029/2012GL051720.

Cao, C., and A. Heidinger, 2002: Inter-comparison of the longwave infrared channels of MODIS and AVHRR/NOAA-16 using simultaneous nadir observations at orbit intersections. *Proc. SPIE*, **4814**, https://doi.org/10.1117/12.451690.

——, M. Weinreb, and H. Xu, 2004: Predicting simultaneous nadir overpasses among polar-orbiting meteorological satellites for the intersatellite calibration of radiometers. *J. Atmos. Oceanic Technol.*, **21**, 537–542, https://doi.org/10.1175/1520-0426(2004)021<0537:PSNOAP>2.0.CO;2.

——, H. Xu, J. Sullivan, L. McMillin, P. Ciren, and Y. Hou, 2005: Intersatellite radiance biases for the High Resolution Infrared Radiation Sounders (HIRS) on board *NOAA-15*, *-16*, and *-17* from simultaneous nadir observations. *J. Atmos. Oceanic Technol.*, **22**, 381–395, https://doi.org/10.1175/JTECH1713.1.

Foelsche, U., S. Syndergaard, J. Fritzer, and G. Kirchengast, 2011: Errors in GNSS radio occultation data: Relevance of the measurement geometry and obliquity of profiles. *Atmos. Meas. Tech.*, **4**, 189–199, https://doi.org/10.5194/amt-4-189-2011.

Griggs, E., E. R. Kursinski, and D. Akos, 2015: Short-term GNSS satellite clock stability. *Radio Sci.*, **50**, 813–826, https://doi.org/10.1002/2015RS005667.

Ho, S.-P., M. Goldberg, Y.-H. Kuo, C.-Z. Zou, and W. Schreiner, 2009: Calibration of temperature in the lower stratosphere from microwave measurements using COSMIC radio occultation data: Preliminary results. *Terr. Atmos. Oceanic Sci.*, **20**, 87–100, https://doi.org/10.3319/TAO.2007.12.06.01(F3C).

——, X. Zhou, Y.-H. Kuo, D. Hunt, and J.-H. Wang, 2010a: Global evaluation of radiosonde water vapor systematic biases using GPS radio occultation from COSMIC and ECMWF analysis. *Remote Sens.*, **2**, 1320–1330, https://doi.org/10.3390/rs2051320.

——, Y.-H. Kuo, W. Schreiner, and X. Zhou, 2010b: Using SI-traceable global positioning system radio occultation measurements for climate monitoring [in ''State of the Climate in 2009'']. *Bull. Amer. Meteor. Soc.*, **91** (7), S36–S37, https://doi.org/10.1175/BAMS-91-7-StateoftheClimate.

——, L. Peng, and H. Voemel, 2017: Characterization of the long-term radiosonde temperature biases in the upper troposphere and lower stratosphere using COSMIC and MetOp-A/GRAS data from 2006 to 2014. *Atmos. Chem. Phys.*, **17**, 4493–4511, https://doi.org/10.5194/acp-17-4493-2017.

——, X. Zhou, S. Kireev, and L. Adhikari, 2019: NESDIS RO science studies and quality assurance through the STAR integrated Cal/Val system: Initial validation of COSMIC-2 data. *IROWG Workshop*, Elsinore, Denmark, IROWG, https://data.cosmic.ucar.edu/gnss-ro/cosmic2/provisional/references/ho_2019.pdf.

——, and Coauthors, 2020: The COSMIC/FORMOSAT-3 radio occultation mission after 12 years: Accomplishments, remaining challenges, and potential impacts of COSMIC-2. *Bull. Amer. Meteor. Soc.*, **101**, E1107–E1136, https://doi.org/10.1175/BAMS-D-18-0290.1.

Hunt, D., S. Sokolovskiy, M. Sleziak-Sallee, T. VanHove, J. P. Weiss, and Z. Zeng, 2019: Paz neutral atmosphere radio occultation retrieval processing. *Seventh IROWG Workshop*, Ellsinore, Denmark, IROWG, https://www.romsaf.org/romsaf-irowg-2019/en/open/1570202090.ca527af47f02b56bd1d9cd50f448ec0d.pdf/Hunt__paz_hv_ro_processing_v03.pdf.

Iacovazzi, R. J., and C. Cao, 2007: Quantifying EOS *Aqua* and NOAA POES AMSU-A brightness temperature biases for weather and climate applications utilizing the SNO method. *J. Atmos. Oceanic Technol.*, **24**, 1895–1909, https://doi.org/10.1175/JTECH2095.1.

Kursinski, E. R., G. A. Hajj, J. T. Schofield, R. P. Linfield, and K. R. Hardy, 1997: Observing the Earth's atmosphere with radio occultation measurements using the global positioning system. *J. Geophys. Res.*, **102**, 23 429–23 465, https://doi.org/10.1029/97JD01569.

Schreiner, W., C. Rocken, S. Sokolovskiy, S. Syndergaard, and D. Hunt, 2007: Estimates of the precision of GPS radio occultations from the COSMIC/FORMOSAT-3 mission. *Geophys. Res. Lett.*, **34**, L04808, https://doi.org/10.1029/2006GL027557.

——, S. Sokolovskiy, D. Hunt, C. Rocken, and Y.-H. Kuo, 2011: Analysis of GPS radio occultation data from the FORMOSAT-3/COSMIC and MetOp/GRAS missions at CDAAC. *Atmos. Meas. Tech.*, **4**, 2255–2272, https://doi.org/10.5194/amt-4-2255-2011.

——, and Coauthors, 2020: COSMIC-2 radio occultation constellation: First results. *Geophys. Res. Lett.*, **47**, e2019GL086841, https://doi.org/10.1029/2019GL086841.

Sokolovskiy, S. V., and Coauthors, 2014: Use of the L2C signal for inversions of GPS radio occultation data in the neutral atmosphere. *GPS Solutions*, **18**, 405–416, https://doi.org/10.1007/s10291-013-0340-x.

Sun, B., A. Reale, S. Schroeder, M. Pettey, and R. Smith, 2019: On the accuracy of Vaisala RS41 versus RS92 upper-air temperature observations. *J. Atmos. Oceanic Technol.*, **36**, 635–653, https://doi.org/10.1175/JTECH-D-18-0081.1.

Wang, L., M. Goldberg, X. Wu, C. Cao, R. Iacovazzi, F. Yu, and Y. Li, 2011: Consistency assessment of Atmospheric Infrared Sounder and Infrared Atmospheric Sounding Interferometer radiances: Double differences versus simultaneous nadir overpasses. *J. Geophys. Res.*, **116**, D11111, https://doi.org/10.1029/2010JD014988.

Weiss, J., 2019: FORMOSAT-7/COSMIC-2 neutral atmosphere provisional data release 1. NOAA Rep., 12 pp., https://data.cosmic.ucar.edu/gnss-ro/cosmic2/provisional/F7C2_NA_Provisional_Data_Release_1_Memo.pdf.

Zou, C.-Z., M. Goldberg, Z. Cheng, N. Grody, J. Sullivan, C. Cao, and D. Tarpley, 2006: Recalibration of Microwave Sounding Unit for climate studies using simultaneous nadir overpasses. *J. Geophys. Res.*, **111**, D19114, https://doi.org/10.1029/2005JD006798.